



An *in situ* inhibition strategy: Forming a physical barrier around ionic crosslinkers to toughen double-network hydrogels



Nannan Jian^a, Jiuling Wang^a, Lei Zuo^{a,*}, Kai Zhang^{a,b,*}

^aSchool of Aerospace Engineering, Beijing Institute of Technology, Beijing 100081, People's Republic of China

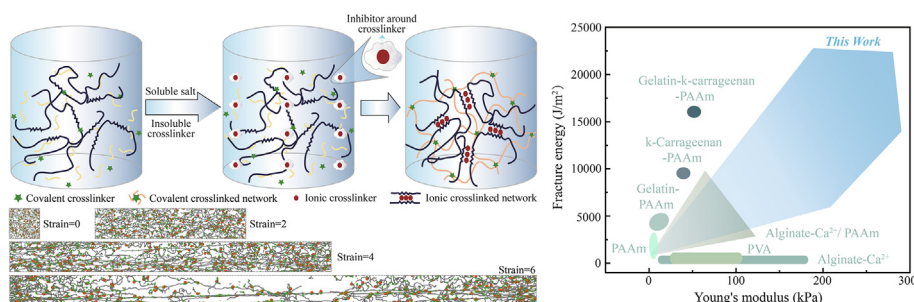
^bTangshan Research Institute, Beijing Institute of Technology, Tangshan 063000, People's Republic of China

HIGHLIGHTS

- An *in situ* inhibition strategy is proposed to toughen double-network (DN) hydrogels in a controllable manner.
- Superior mechanical properties of DN hydrogels are obtained via our *in situ* inhibition strategy.
- Our *in situ* inhibition strategy has great potential to become a general approach to toughen DN hydrogels.

GRAPHICAL ABSTRACT

We propose a general *in situ* inhibition method to toughen the DN hydrogels. It is achieved by generating inhibitor *in situ* to form a physical barrier around the ionic crosslinker, thereby impeding the release of crosslinking ions. Using molecular dynamics simulations, it is revealed that decreasing the ionic crosslinking rate can contribute to an improvement in the homogeneity and mechanical properties. For alginate-Ca²⁺/PAAm DN hydrogels, the fracture energy obtained by this method is notably larger than the previously reported values.



ARTICLE INFO

Article history:

Received 1 October 2022

Revised 12 December 2022

Accepted 19 December 2022

Available online 20 December 2022

Keywords:

Double-network (DN) hydrogels

Homogeneity

Ionic crosslinking density

Inhibitor

Toughness

ABSTRACT

Ionically crosslinked networks are extremely effective in reinforcing double-network (DN) hydrogels. But the simultaneous improvement of both homogeneity and ionic crosslinking density remains as a challenge for toughening DN hydrogels. Herein, an *in situ* inhibition method is proposed to solve this problem. In this method, inhibitor is generated *in situ* to form a physical barrier around the ionic crosslinker, thereby decreasing the ionic crosslinking rate and further toughening DN hydrogels in a controllable manner. The chemical structure, micromorphology and mechanical properties were investigated, and molecular dynamics simulations were performed to reveal the inhibition mechanism. The transmission electron microscopy (TEM) images confirm the formation of inhibitors. It is revealed that the introduction of inhibitor can decrease ionic crosslinking rate, leading to an improvement in homogeneity and mechanical properties. The fracture energy of alginate-Ca²⁺/polyacrylamide (PAAm) DN hydrogels is up to 19,638 ± 947 J/m², which is notably larger than the previously reported values (9000–16,000 J/m²). The inhibitor does not affect the chemical structures, thermal stability and micromorphology. This *in situ* inhibition method has significant potential to become a general method to toughen DN hydrogels containing ionically crosslinked networks, which will greatly promote the usage of hydrogels in diverse engineering applications.

© 2023 The Authors. Published by Elsevier Ltd. This is an open access article under the CC BY-NC-ND license (<http://creativecommons.org/licenses/by-nc-nd/4.0/>).

* Corresponding authors at: School of Aerospace Engineering, Beijing Institute of Technology, Beijing 100081, People's Republic of China (K. Zhang).

E-mail addresses: zuolei@bit.edu.cn (L. Zuo), zhangkai@bit.edu.cn (K. Zhang).

1. Introduction

Recently, hydrogels have been employed as structural materials for wearable electronics [1–5], scaffolds [6–8], soft robotics [9–12], underwater communication [13] and so on. However, these load-bearing hydrogels are often limited by their poor mechanical properties. The double-network (DN) strategy is effective in toughening hydrogels by building a brittle network into a stretchy polymer network [4,14–17]. During deformation, the brittle network fragments into small clusters to dissipate vast energy, whereas the stretchy polymer network entangles with the clusters and maintains the integrity of the hydrogel [4,14–17]. Suo et al. [14] synthesized a family of tough and stretchable alginate- Ca^{2+} /polyacrylamide (PAAm) DN hydrogels. Although such hydrogels contain ~ 86 wt.% water, they display excellent mechanical properties with a breaking strain of up to 2100 % and a fracture energy of up to 9000 J/m². Wu et al. [17] prepared κ -carrageenan/PAAm DN hydrogels, which are achieved by using zirconium ions (Zr^{4+}) to further crosslink the first physical network of κ -carrageenan. These DN hydrogels display remarkable mechanical performances with breaking strains of 300–2200 %, tensile breaking stress of 1.5–3.2 MPa, Young's modulus of 0.2–2.2 MPa and fracture energies of 400–18,500 J/m². The value of 18,500 J/m² is the highest one reported for hydrogels with high water contents of 83–91 wt.%.

A relatively high ionic crosslinking density is desired for increased toughening of DN hydrogels [18]. However, the ionic crosslinking rate is so fast that any attempt to significantly raise the crosslinking density is frustrated by the high viscosity, making it difficult to form a homogeneous hydrogel. As shown in Fig. 1A, once the ionic crosslinker is added, local gelation will immediately occur. The newly formed hydrogel will rapidly wrap around the surface of ionic crosslinker. As a result, ionic crosslinker cannot be dispersed evenly, which leads to irregular hydrogel lumps. During the stretching of these inhomogeneous hydrogels, regions with fewer crosslinks will become so weak that vast energy cannot be dissipated when cracks initiate or propagate to these regions, resulting in a declined toughness [14]. Thus, the simultaneous

improvement of both homogeneity and ionic crosslinking density remains a challenge for toughening DN hydrogels.

Two methods have been used to overcome the adverse effects of the rapid ionic crosslinking rate. The first method is the one-step synthesis by incorporating a slow-release ionic crosslinker [14,19,20]. The second method is multi-step polymerization by first forming a pre-gel network and then soaking in an ionic solution to further form the ionically crosslinked network [17,18,21]. Suo et al. [14] has used the first method to improve the homogeneity of tough and stretchable alginate- Ca^{2+} /PAAm DN hydrogels by employing insoluble CaSO_4 as crosslinker. To avoid the adverse effects of the rapid crosslinking rate between alginate and CaSO_4 , Suo et al. creatively using two syringes to push against each other to form a strong shear flow, which effectively accelerates the homogenization of the pre-gel solution [14]. However, the concentrations of the ionic crosslinker CaSO_4 in these hydrogels are low. The optimal ratio of CaSO_4 was fixed at only 0.1328 that of alginate, which limits the further improvement of mechanical properties of these alginate- Ca^{2+} /PAAm DN hydrogels. Besides, it is difficult to synthesize a large-size sample by the rapid-shear method. In order to achieve a controllable and slower crosslinking rate, glucono-d-lactone (GDL) has been employed as a gelation-triggering agent to slowly release Ca^{2+} from insoluble CaCO_3 or soluble EDTA- Ca [19–21]. Several homogeneous alginate- Ca^{2+} single-network (SN) hydrogels have been prepared by this method. However, so far, there are no relevant research on DN hydrogel based on GDL. Although the above strategies can improve the homogeneity to some extent, none of them can achieve a sufficiently high crosslinking density under the condition of high uniformity, especially for the fabrication of hydrogels with a large size.

The second method has been employed to increase the ionic crosslinking density of DN hydrogels [17,18]. Suo and co-workers [18] increase the ionic crosslinking density of alginate network by soaking the alginate/PAAm pre-gels in a large volume of CaCl_2 solution for at least 3 days. These alginate- Ca^{2+} /PAAm DN hydrogels display a significant improvement of fracture energies up to $\sim 16,000$ J/m². Similarly, zheng et al. [17] obtained a series of

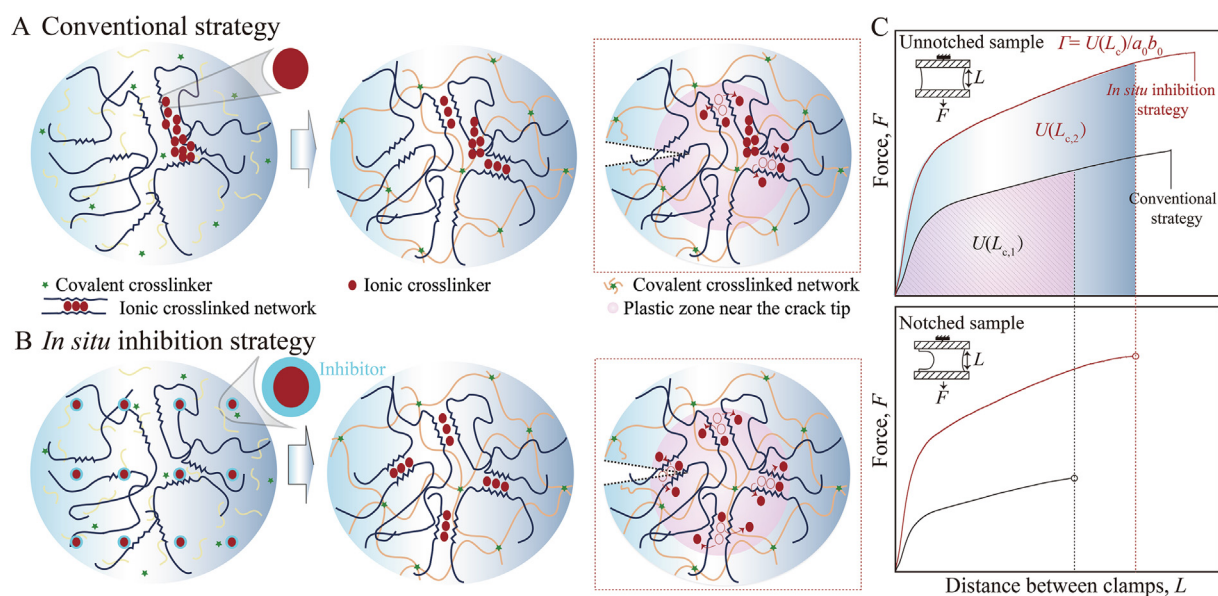


Fig. 1. Design principles for toughening DN hydrogels. Schematic diagram of the conventional strategy (A) and *in situ* inhibition strategy (B) for the preparation of DN hydrogels. (C) Experimental determination of fracture energy for DN hydrogels formed by the two different strategies. An unnotched sample was used to measure the force-length curve. The area beneath the force-length curve gave the work done by the force to the unnotched sample, $U(L)$. The notched sample was used to measure the critical distance between the clamps, L_c , when the notch turned into a running crack. $L_{c,1}$ and $L_{c,2}$ represent the critical distance of the samples prepared by the conventional and *in situ* inhibition strategies, respectively. a_0 and b_0 represent the width and thickness of the samples, respectively.

κ -carrageenan-Zr⁴⁺/PAAm DN hydrogels by this method. These hydrogels display remarkable mechanical performances with the fracture energies of up to $\sim 18,500 \text{ J/m}^2$ [18]. The second method effectively bypasses the problem of inhomogeneous mixing. However, compared to the one-step method, the second method is relatively complicated and time consuming. Furthermore, the hydrogel shape and geometric size changed significantly during soaking process. It is of great significance to develop a simple and universal method to prepare DN hydrogels with high homogeneity and ionic crosslinking density, and precise shape and size.

In this work, an *in situ* inhibition strategy was proposed to toughen classic alginate-Ca²⁺/PAAm DN hydrogels by slowing the ionic crosslinking rate controllably. During the preparation of these DN hydrogels, inhibitor was formed *in situ* to provide a physical barrier around the ionic crosslinker, thereby hindering the release of crosslinking Ca²⁺ and obtaining homogeneous hydrogels with high ionic crosslinking density. The chemical structure, microstructure, thermal degradation and mechanical properties (especially the crack resistance) of these hydrogels were investigated systematically. Besides, molecular dynamics simulations were performed. This method can be readily extended to other ionically crosslinked networks and open a new avenue for the development of DN hydrogels with outstanding mechanical properties.

2. Experimental section

2.1. Materials

Precursor acrylamide (AAM, AR, 99.0 %, Sigma-Aldrich), covalent crosslinker *N,N*-methylene diacrylamide (MBAA, AR, 97 %, Alfa Aesar), photoinitiator/thermal initiator ammonium persulphate (APS, AR, ≥ 98.0 %, Sigma-Aldrich), catalyst *N,N,N,N*-tetramethylethylenediamine (TEMED, AR, >98.0 %, Sigma-Aldrich), sodium alginate (AR, viscosity of $200 \pm 20 \text{ mpa.s}$, Sigma-Aldrich), ionic crosslinker two hydrated calcium sulfate (CaSO₄·2H₂O, AR, 99.0 %, Sigma-Aldrich), additive sodium pyrophosphate (Na₄P₂O₇, AR, 99.0 %, Sigma-Aldrich), additive sodium carbonate (Na₂CO₃, AR, 99.0 %, Sigma-Aldrich), additive sodium citrate (Na₃C₆H₅O₇·2H₂O, AR, 99.0 %, Sigma-Aldrich), additive disodium oxalate (Na₂C₂O₄, AR, 99.0 %, Sigma-Aldrich) and nano superhydrophobic self-cleaning coating (ZXL-CSS, Shandong Laiyang Zixilai Environmental Protection Technology Co., Ltd.) were purchased from commercial chemical reagent companies and used directly without further purification. Ultrapure (UP) water was made using a UP water machine (UPH-I-10 T).

2.2. Preparation of alginate-Ca²⁺/PAAm DN hydrogels

The alginate-Ca²⁺/PAAm DN hydrogels were prepared by using our strategy to controllably tune the ionic crosslinking rate. The procedures are as follows. (1) Preparation of 0.023 wt.% MBAA solution: 0.023 g of MBAA powder were added to 10 mL of UP water until a homogeneous solution was formed. (2) Preparation of 0.2 M APS solution: 0.456 g of APS powder were added to 10 mL of UP water until a homogeneous solution was formed. (3) Preparation of pre-gel solution: Prescribed amounts of sodium alginate and AAM were dissolved in UP water at room temperature to obtain a homogeneous and transparent solution. Prescribed amounts of 0.023 wt.% MBAA solution, 0.2 M APS solution, TEMED and Na₄P₂O₇/Na₂CO₃/Na₃C₆H₅O₇·2H₂O/Na₂C₂O₄ were added to the above solution and stirred at the same temperature for 10 min. Prescribed amounts of CaSO₄·2H₂O and UP water were then added to the reaction mixture and stirred at the same temperature for 5 min to obtain a pre-gel solution. (4) The pre-gel solution was treated with a mixing deaerator (SBT-TPJ-003) for 1 min to remove

air bubbles. (5) The defoamed pre-gel solution was poured into a homemade acrylic mold of $75.0 \times 150.0 \times 3.0 \text{ mm}^3$ and placed for 1 h to remove bubbles. A glass plate (3 mm thick) coated with a nano superhydrophobic self-cleaning coating was then used as a coverslip. The pre-gel solution was irradiated under UV light at room temperature for 1 h (with a 15 W power, 254 nm wavelength and $1.2 \times 10^4 \text{ } \mu\text{J/cm}^2$ energy density using a UV crosslinkers XL-1500, Spectronics) to form the first network of PAAm and obtain the as-prepared hydrogel. (6) The as-prepared hydrogel was kept at room temperature for 24 h to ensure the complete formation of the second alginate-Ca²⁺ hydrogel network.

2.3. Viscosity characterization

The viscosity of the pre-gel solution was measured at room temperature using a rotary viscometer (LC-NDJ-99 T, Lichen, China) with a shear rate of 1.24 s^{-1} .

2.4. Fourier transform infrared (FT-IR) analysis

Fourier transform infrared (FT-IR) spectroscopy (Nicolet iS5, Thermo Scientific, USA) with potassium bromide (KBr) as the internal reference was used to characterize the chemical structures of alginate-Ca²⁺ SN hydrogels and alginate-Ca²⁺/PAAm DN hydrogels with soluble sodium salts. The soluble sodium salts were Na₄P₂O₇, Na₂CO₃, Na₃C₆H₅O₇·2H₂O and Na₂C₂O₄. The alginate-Ca²⁺ SN hydrogels and alginate-Ca²⁺/PAAm DN hydrogels without soluble sodium salts were also prepared by the conventional method. The weight ratios of alginate to AAM for the alginate-Ca²⁺/PAAm DN hydrogels were 3:11. The hydrogels were dried at 60 °C for 24 h in a vacuum oven (ZKGT-6053, AODEMA, China) and ground into powders before characterization.

2.5. Thermogravimetric (TGA) analysis

The components and thermal degradation behaviors of the alginate-Ca²⁺ SN and alginate-Ca²⁺/PAAm DN hydrogels with soluble sodium salts were studied using a thermal gravimetric analyzer (PE STA8000) under a nitrogen atmosphere with a heating rate of 10 °C/min and a nitrogen rate of 40 mL/min. The soluble sodium salts were Na₄P₂O₇, Na₂CO₃, Na₃C₆H₅O₇·2H₂O and Na₂C₂O₄. The alginate-Ca²⁺ SN and alginate-Ca²⁺/PAAm DN hydrogels without soluble sodium salts were also prepared by the conventional method. Samples were scanned from 30 to 800 °C. The weight ratio of alginate to AAM was 3:11 for the alginate-Ca²⁺/PAAm DN hydrogels. These hydrogels were dried at 60 °C for 24 h in a vacuum oven (ZKGT-6053, AODEMA, China) and then ground in a mortar. Samples weighing between 4 and 8 mg were tested in crucibles.

2.6. Cryo-scanning electron microscopy (cryo-SEM) imaging

Cryo-scanning electron microscopy (cryo-SEM) imaging was conducted by employing a low-vacuum Quanta 450 SEM (FEI Company, Hillsboro, OR, USA) with a cryogenic freezing preparation transfer system (PP3000T, Quorum company, UK) as attachment. Small pieces were first cut from the samples with a pair of scissors and fixed on the sample stage by using conductive carbon glue as binder. To freeze the samples, they were then plunged into nitrogen slush on the Quorum preparation bench. The frozen samples were further transferred to the cryo-preparation chamber and freeze fractured. All samples were sputtered with gold for 60 s in an argon atmosphere to guarantee sufficient electrical conductivity. Before imaging, each sample was sublimated at $-90 \text{ }^\circ\text{C}$ for 10 min on the cold stage in the SEM chamber. Imaging was con-

ducted at a temperature of $-140\text{ }^{\circ}\text{C}$ and an accelerating voltage of 10 kV.

2.7. Transmission electron microscopy (TEM) imaging of particles

Transmission electron microscopy (TEM) was used to visualize the CaSO_4 , $\text{Ca}_2\text{P}_2\text{O}_7$ and $\text{CaSO}_4\text{-Ca}_2\text{P}_2\text{O}_7$ mixture. (1) Preparation of CaSO_4 suspension: The 0.19 g of $\text{CaSO}_4\cdot 2\text{H}_2\text{O}$ powder were added to 20 mL of UP water. (2) Preparation of $\text{Ca}_2\text{P}_2\text{O}_7$ suspension: The 0.19 g of $\text{CaSO}_4\cdot 2\text{H}_2\text{O}$ and 0.15 g of $\text{Na}_4\text{P}_2\text{O}_7$ were added into 10 mL of UP water to obtain the CaSO_4 suspension and $\text{Na}_4\text{P}_2\text{O}_7$ solution, respectively. The homogeneous and transparent CaSO_4 solution was obtained by filtration of the CaSO_4 suspension, which was then mixed with the $\text{Na}_4\text{P}_2\text{O}_7$ solution to obtain the $\text{Ca}_2\text{P}_2\text{O}_7$ suspension. (3) Preparation of $\text{CaSO}_4\text{-Ca}_2\text{P}_2\text{O}_7$ mixture: The 0.15 g of $\text{Na}_4\text{P}_2\text{O}_7$ powder were added to 20 mL of UP water until a homogeneous solution was formed. Then, 0.81 g of $\text{CaSO}_4\cdot 2\text{H}_2\text{O}$ powder were added to the solution. It is noted that CaSO_4 is superfluous. The suspension was then drop-cast on holey carbon-coated TEM grids. The TEM grids were stored in a desiccator for 1 d to remove the water. The images were collected using a high-resolution transmission electron microscope (JEOL JEM-F200) at an acceleration voltage of 200 kV.

2.8. Molecular dynamics (MD) simulations

Coarse-grained molecular dynamics (CGMD) simulations were performed to investigate the effect of the ionic crosslinking rate on the spatial distribution of ionic crosslinks in the hydrogel using a bead-spring model [21–23]. The initial box size is $82.6\sigma \times 82.6\sigma \times 82.6\sigma$ (σ is the unit of length) and periodic boundary conditions are applied in the simulation. The system is composed of 480 polymer chains with chain length $N = 200$ and 3600 crosslinkers, and there are 99,600 beads in the system with a number density of $\rho = 0.17\sigma^{-3}$. The polymer chains are used to model the alginate chains and 12 % of the polymer beads are set up as active beads to model the G units in the alginate chains. One Lennard-Jones bead is used to model the crosslinker. The crosslinker can react with the active beads in the polymer chains. The interaction between all beads of mass m and size σ is described by the Weeks–Chandler–Andersen (WCA) potential in Eq. (1):

$$U_{WCA}(r) = \begin{cases} 4\varepsilon \left[\left(\frac{\sigma}{r}\right)^{12} - \left(\frac{\sigma}{r}\right)^6 - \left(\frac{\sigma}{r_c}\right)^{12} + \left(\frac{\sigma}{r_c}\right)^6 \right], & r \leq r_c \\ 0, & r > r_c \end{cases} \quad (1)$$

where the cutoff distance $r_c = 2^{1/6}\sigma$ and ε is the unit of energy in Eq. (1). The characteristic timescale in the simulation is $\tau = \sigma\sqrt{m/\varepsilon}$. The bonds between neighboring polymer beads are modeled by the finite extensible nonlinear elastic (FENE) potential in Eq. (2):

$$U_{FENE}(r) = \begin{cases} -\frac{k}{2}R_0^2 \ln \left[1 - \left(\frac{r}{R_0}\right)^2 \right], & r < R_0 \\ \infty, & r \geq R_0 \end{cases} \quad (2)$$

where the force constant $k = 30\varepsilon/\sigma^2$ and the maximum bond length $R_0 = 1.5\sigma$ in Eq. (2). In addition, adjacent bonds are coupled by a bond bending potential in Eq. (3):

$$U_{bend}(\theta) = k_\theta(1 - \cos\theta) \quad (3)$$

where $k_\theta = 1.5\varepsilon$ and θ is the angle between the two bonds in Eq. (3). The Nosé–Hoover thermostat is used to control the temperature at $T = 1.0\varepsilon/k_B$, where k_B is the Boltzmann constant, with the damping parameter 10τ . The velocity Verlet algorithm was utilized to perform the time integration with a time step 0.01τ . All simulations were performed with the LAMMPS package [24].

At the beginning of the simulation, the ionic crosslinkers are arranged in eight clusters to model the inhomogeneous mixing of Ca^{2+} with the pre-gel solution in experiments, as shown in Fig. 3B. In the simulation, when one crosslinker encounters the G unit, a bond is formed with probability p . The newly formed bond is also described by Eq. (2). A crosslinker can bond with up to two G units and a G unit can only bind to one crosslinker. We set p to 1.0, 10^{-1} , 10^{-2} and 10^{-3} to simulate different ionic crosslinking rates. We continue the simulation until all crosslinkers bond to two G units. The above simulation method allows us to obtain hydrogel samples at different crosslinking rates.

To study the effect of spatial distribution of ionic crosslinks on the mechanical properties of hydrogels, uniaxial tensile simulations along the z -direction on the obtained model hydrogel samples were also studied. To simulate the mechanical failure of polymer chains and crosslinks, the FENE bonding potential is replaced by the breakable quartic potential in Eq. (4) [25–27]:

$$U_{quartic}(r) = k_1(r - R_1)^3(r - R_2) \quad (4)$$

where $k_1 = 2351\varepsilon/\sigma^4$, $R_1 = 1.5\sigma$ and $R_2 = 0.7575\sigma$ in Eq. (4). Both bonds along the backbone of the polymer and the crosslinks can break in the simulations. The uniaxial tensile simulations were performed at a constant strain rate of $1 \times 10^{-3}/\tau$ while keeping the volume of the simulation box constant (we assume that the Poisson's ratio of the hydrogel is 0.5). Our results show that reducing the strain rate by one order of magnitude does not significantly alter the mechanical response of the hydrogels. We recorded the normal stress σ_x , σ_y and σ_z as a function of the engineering strain $\lambda = L_z/L_z^0 - 1$, where L_z is the box size along the z -direction and L_z^0 is the initial box size. The deviatoric (true) stress along the z -direction is calculated as $\sigma_{true} = \sigma_z - (\sigma_x + \sigma_y)/2$ and the engineering stress along the z -direction is calculated as $\sigma_{eng} = \sigma_{true}/(\lambda + 1)$.

2.9. Determination of fracture energy

The fracture energy Γ of the hydrogels was measured by adopting the method introduced by Rivlin and Thomas [28]. For an extremely stretchable hydrogel, the method needs to be adapted to determine its fracture energy by pulling two samples of the same hydrogel separately. One sample was unnotched and it was pulled to acquire the work done by the applied force, $U(L)$. L was the distance between the two clamps. The other sample was notched. During pulling, when the notch turned into a running crack, the critical distance between the clamps L_c was identified, and the fracture energy Γ was further calculated from the Eq. (5):

$$\Gamma = U(L_c)/a_0b_0 \quad (5)$$

Thus, the ‘‘Fracture energy’’ is the properties of the material itself.

A tensile machine (WDW-2, Changchun Kexin Test, China) was used to conduct the mechanical tests with a stretching rate of 2 min^{-1} at room temperature and in air. The load cell was 2 kN. Hydrogel samples were glued to two acrylic clamps ($90.0 \times 40.0 \times 3.0\text{ mm}^3$) using Loctite 435 as the adhesive. For an undeformed hydrogel sample, its width was $a_0 = 75\text{ mm}$, and the thickness was $b_0 = 3\text{ mm}$. In the undeformed state before stretching, the initial distance between the two clamps was $L_0 = 5\text{ mm}$. The notched sample was obtained using a razor blade. Canon 90D camera was used to record the stretching process of the notched sample.

3. Results and discussion

3.1. Mechanism of *in situ* inhibition method

An *in situ* inhibition method (Fig. 1B) was proposed to toughen DN hydrogels. It is achieved by generating a substance known as inhibitor *in situ* to form a physical barrier around the ionic crosslinker. The barrier can impede the release of crosslinking ions and thus decrease ionic crosslinking rate. The decreased ionic crosslinking rate provides a sufficient time for the uniform dispersion of the ionic crosslinker before gelation, thereby facilitating the preparation of DN hydrogels with high uniformity and ionic crosslinking density. Therefore, during the stretch of a notched hydrogel, vast energy will be dissipated by unzipping the ionic network of high crosslinking density, leading to an improved toughness (Fig. 1C).

Specifically, the classic alginate- Ca^{2+} /PAAm DN hydrogels were employed as the research objects. A soluble salt, $\text{Na}_4\text{P}_2\text{O}_7$, was introduced into the alginate-AAm mixture solution before adding the crosslinker CaSO_4 (Fig. 2A). When Ca^{2+} is added into the $\text{Na}_4\text{P}_2\text{O}_7$ -alginate mixture, two reactions occur simultaneously: 1) Crosslinking reaction of alginate and Ca^{2+} ; 2) Complexation reaction of $\text{Na}_4\text{P}_2\text{O}_7$ and Ca^{2+} . However, the newly formed alginate- Ca^{2+} hydrogel will dissolve due to that $\text{Na}_4\text{P}_2\text{O}_7$ can capture Ca^{2+} from alginate- Ca^{2+} hydrogel network, which is called de-crosslinking. This phenomenon of de-crosslinking has been verified by previous literature [29] and our experiment (Figure S1). Thus, $\text{Na}_4\text{P}_2\text{O}_7$ will capture the crosslinking Ca^{2+} in preference to the alginate apparently as long as $\text{Na}_4\text{P}_2\text{O}_7$ exists. The newly formed $\text{Ca}_2\text{P}_2\text{O}_7$, acting as an inhibitor, is generated *in situ* to form a physical barrier around CaSO_4 to impede the release of Ca^{2+} and decrease the ionic crosslinking rate. The reduced ionic crosslinking rate will provide enough time for the uniform dispersion of CaSO_4 , which is conducive to the formation of uniform pre-gel solution. The dispersion states of pre-gel solution with and without $\text{Na}_4\text{P}_2\text{O}_7$ can be intuitively confirmed by the corresponding photographs of the alginate- Ca^{2+} SN hydrogels (Fig. 2B). It can be seen that the hydrogel prepared without $\text{Na}_4\text{P}_2\text{O}_7$ displays a rugged structure, while the hydrogel with $\text{Na}_4\text{P}_2\text{O}_7$ exhibits a smooth surface. These obvious visual differences proves that the inhibitor $\text{Ca}_2\text{P}_2\text{O}_7$ can improve the homogeneity of the ionic crosslinked hydrogels, which is expected to further improve the mechanical properties of hydrogels.

To quantitatively characterize the inhibition effect of our proposed *in situ* inhibition strategy, the viscosity variations of the pre-gel solutions with different $\text{Na}_4\text{P}_2\text{O}_7$ contents (Fig. 2C and S2) were also investigated in detail. The initial viscosity of the pre-gel solution is defined as the viscosity measured after CaSO_4 was added and stirred for 5 min. As shown in Fig. 2C, it can be seen that the viscosities of the pre-gel solutions with $\text{Na}_4\text{P}_2\text{O}_7$ are obviously lower than that of the pre-gel solution without $\text{Na}_4\text{P}_2\text{O}_7$. It can also be seen that the pre-gel solutions with $\text{Na}_4\text{P}_2\text{O}_7$ have lower initial viscosities of 4687–5342 cp, which is only 13 % of the viscosity of the pre-gel solution without $\text{Na}_4\text{P}_2\text{O}_7$ (~41,668 cp). The difference in viscosity of these pre-gel solutions directly proved that the introduction of $\text{Na}_4\text{P}_2\text{O}_7$ really reduced the ionic crosslinking rate. It should be noted that the viscosity of the pre-gel solution with $\text{Na}_4\text{P}_2\text{O}_7$ remains almost unchanged until 12 min when the weight ratio of $\text{Na}_4\text{P}_2\text{O}_7$ to CaO_4 exceeds 23.53 wt.%, meaning that there is almost no hydrogel formation in the pre-gel solution within 12 min, which is mainly attributed to the inhibition effect of the newly formed $\text{Ca}_2\text{P}_2\text{O}_7$. As a result, compared with the conventional method for the preparation of alginate- Ca^{2+} /PAAm DN hydrogels, *in situ* strategy can decrease the ionic crosslinking rate and leave a sufficient time for the uniform dispersion of CaSO_4 in the pre-gel solutions before gelation.

Furthermore, the inhibition effect can be enhanced by an increase in the amount of $\text{Na}_4\text{P}_2\text{O}_7$ (Fig. 2C and Figure S2). In these experiments, it was found that when the viscosity exceeds 30,000 cp, the pre-gel solution has almost no fluidity, indicating that the gelation is basically complete. Therefore, the time corresponding to the viscosity of 30,000 cp was defined as the gelation time. With increasing the $\text{Na}_4\text{P}_2\text{O}_7$ content from 0 wt.% to 28.22 wt.%, the gelation time shows an obvious increase from ~0 min to ~25 min, which is attributed to the increase of the newly formed $\text{Ca}_2\text{P}_2\text{O}_7$ content. The higher content of $\text{Na}_4\text{P}_2\text{O}_7$, the lower ionic crosslinking rate. Lower ionic crosslinking rate provides the possibility to increase the concentration of ionic crosslinking agent CaSO_4 , which is expected to further improve the ionic crosslinking density of alginate- Ca^{2+} /PAAm DN hydrogels and toughen them. The amount of the crosslinker CaSO_4 through our *in situ* inhibition method can be at least increased to around five times that from the conventional method [14]. However, the amount of $\text{Na}_4\text{P}_2\text{O}_7$ added should not be excessive (Figure S2) because the ionic crosslinking density of the hydrogel will decrease due to the increased consumption of CaSO_4 by $\text{Na}_4\text{P}_2\text{O}_7$. Furthermore, an excessively prolonged gelation time will lead to the sedimentation of CaSO_4 particles, which will inevitably decrease the homogeneity of the hydrogel (Figure S2).

Transmission electron microscopy (TEM) was conducted to confirm the formation of the physical barrier that can impede the release of crosslinking ions. As shown in Fig. 2D and E, the CaSO_4 particles display a needle-like structure, while $\text{Ca}_2\text{P}_2\text{O}_7$ displays a circular-like structure. The product of the reaction between $\text{Na}_4\text{P}_2\text{O}_7$ and CaSO_4 shows a hazy structure (Fig. 2F), which is completely different from the structures of CaSO_4 and $\text{Ca}_2\text{P}_2\text{O}_7$ (Fig. 2D and E). In these hazy substances, $\text{Ca}_2\text{P}_2\text{O}_7$ is formed around CaSO_4 to serve as a physical barrier to impede the release of crosslinking Ca^{2+} . In addition, the chemical structures (Figure S3), thermal degradation stability (Figure S4) and micromorphology (Figure S5) of alginate- Ca^{2+} SN and alginate- Ca^{2+} /PAAm DN hydrogels with and without $\text{Na}_4\text{P}_2\text{O}_7$ have also been investigated. These results show that the hydrogels prepared by our *in situ* inhibition method display similar chemical and physical properties with the hydrogels prepared by the conventional method, which indicates that the addition of $\text{Na}_4\text{P}_2\text{O}_7$ does not affect the chemical and physical properties of the hydrogel network.

3.2. Clarification of toughening effect by molecular dynamics simulations

To understand how the ionic crosslinking rate affects the uniformity of the spatial distribution of ionic crosslinks in the hydrogel and further affects the mechanical properties of the hydrogel, coarse-grained molecular dynamics (CGMD) simulations were performed. A model system composed of polymer chains and ionic crosslinkers was constructed to model the alginate chains and Ca^{2+} , as shown in Fig. 3A. A total of 12 % of the polymer beads were set up as active beads to mimic the G units in the alginate chains and these active beads could form bonds with ionic crosslinker. To mimic the inhomogeneous mixing of Ca^{2+} with the pre-gel solution, the ionic crosslinkers were placed in eight clusters (Fig. 3B). The crosslinkers can diffuse and react with the G units in the polymer chains. The reaction probability p when one crosslinker encounters the G unit can be tuned to simulate the different ionic reaction rates in the experiments. Fig. 3C shows the snapshots of the distribution of crosslinks in the formed hydrogels for $p = 1.0, 10^{-1}, 10^{-2}$ and 10^{-3} , respectively. When $p = 1$, the crosslinkers react rapidly with the neighboring G units, resulting in a heterogeneous distribution of crosslinks in the hydrogel (Fig. 3C). With decreasing p , the crosslinkers can diffuse and be evenly distributed in the system before reacting with the G units. Consequently, the distribution of crosslinks in

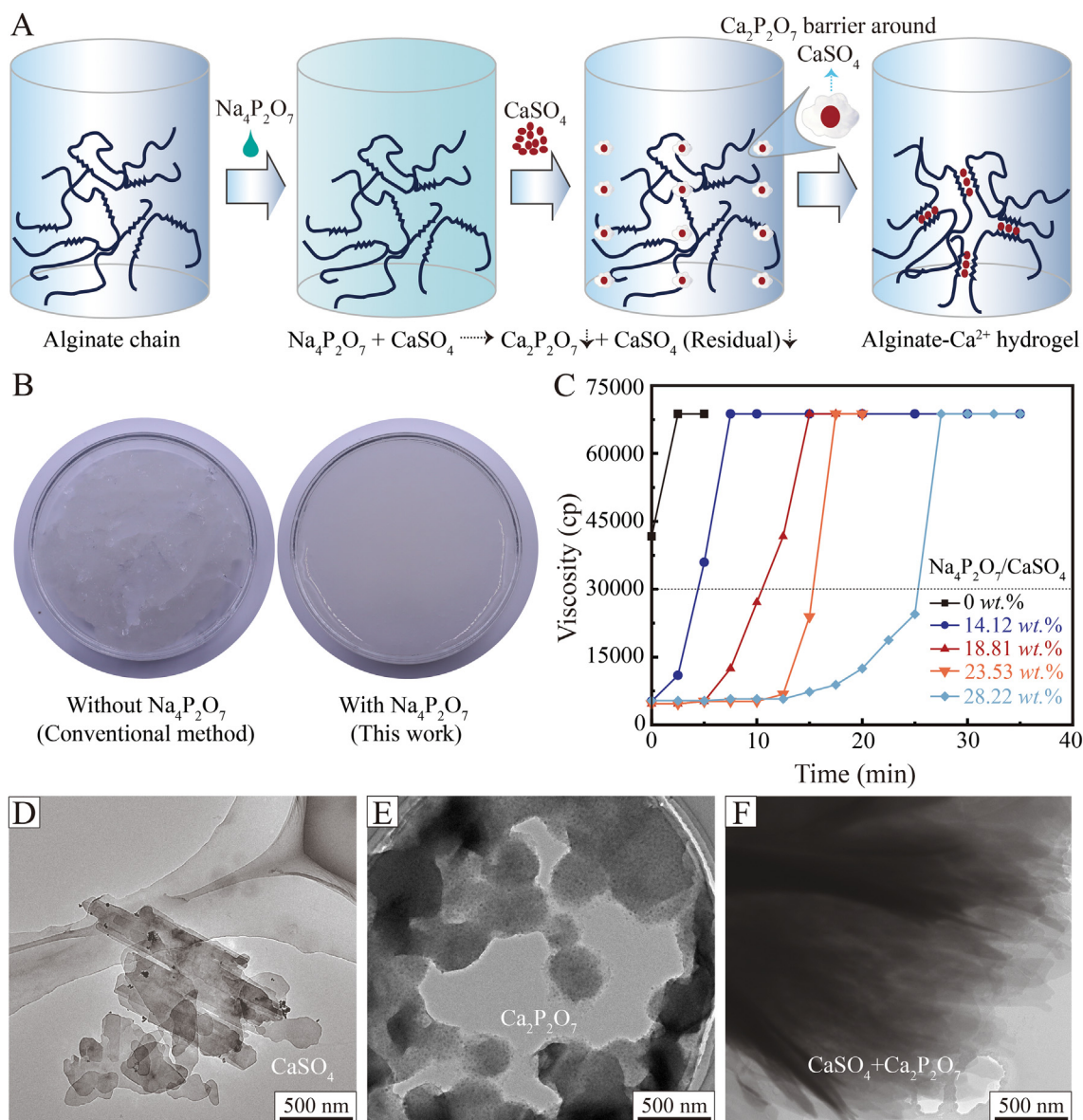


Fig. 2. Mechanism of the *in situ* inhibition method. (A) Schematic diagram of the *in situ* inhibition method for the preparation of alginate- Ca^{2+} SN hydrogels with high uniformity and ionic crosslinking density. (B) Photographs of alginate- Ca^{2+} SN hydrogels formed by the conventional and *in situ* inhibition methods. (C) Viscosity-time curves of the pre-gel solutions for alginate- Ca^{2+} SN hydrogels with various weight ratios of $\text{Na}_4\text{P}_2\text{O}_7$ to CaSO_4 . The water content was fixed at 97.00 wt.%. The weight ratio of CaSO_4 was fixed at 81.25 wt.% that of alginate. The weight ratio of $\text{Na}_4\text{P}_2\text{O}_7$ was fixed at 18.81 wt.% that of CaSO_4 for Fig. 2B. Representative TEM images of (D) CaSO_4 , (E) $\text{Ca}_2\text{P}_2\text{O}_7$ and (F) the product of the reaction between $\text{Na}_4\text{P}_2\text{O}_7$ and CaSO_4 .

the hydrogel is more uniform (Fig. 3C). These simulation results demonstrate that reducing the crosslinking rate is an effective method to obtain uniformly crosslinked hydrogels.

How the spatial distribution of ionic crosslinks affects the mechanical properties of hydrogels was further investigated. Uniaxial tensile simulations on the obtained model hydrogel samples were performed and the engineering stress-strain behavior of the hydrogels is shown in Fig. 3D (see methods for the calculation of stress and strain). The area under the stress-strain curve (energy per unit volume before failure, U) was used to characterize the toughness of the hydrogel. With increasing uniformity of the crosslinks, the U value increases and the U value at $p = 10^{-3}$ ($1.35\varepsilon/\sigma^3$) is more than double that at $p = 1.0$ ($0.65\varepsilon/\sigma^3$) (Fig. 3E). The high toughness at $p = 10^{-3}$ is attributed to the high strain at rupture. At $p = 1.0$, the hydrogel fails at a strain of 3; however, at $p = 10^{-3}$, the hydrogel fails at a strain of 6 (Fig. 3F). In fact, there

are regions with low and high crosslinking density in the non-uniformly crosslinked hydrogels. In these regions with fewer crosslinks, cracks are prone to develop under small strains, which further causes the failure of the hydrogels. These results indicate that improving the uniformity of ionic crosslinks in hydrogels can significantly enhance their mechanical properties. In experiments, the release rate of Ca^{2+} was successfully reduced by generating an inhibitor $\text{Ca}_2\text{P}_2\text{O}_7$ around CaSO_4 , which further slowed down the ionic crosslinking rate and allowed us to obtain hydrogels with high uniformity. Combined with the results of molecular dynamics simulations, it is expected that these hydrogels can achieve a high toughness.

3.3. Experimental verification of toughening effect

These alginate- Ca^{2+} /PAAm DN hydrogels prepared by the *in situ* inhibition method display extremely high stretchability and tough-

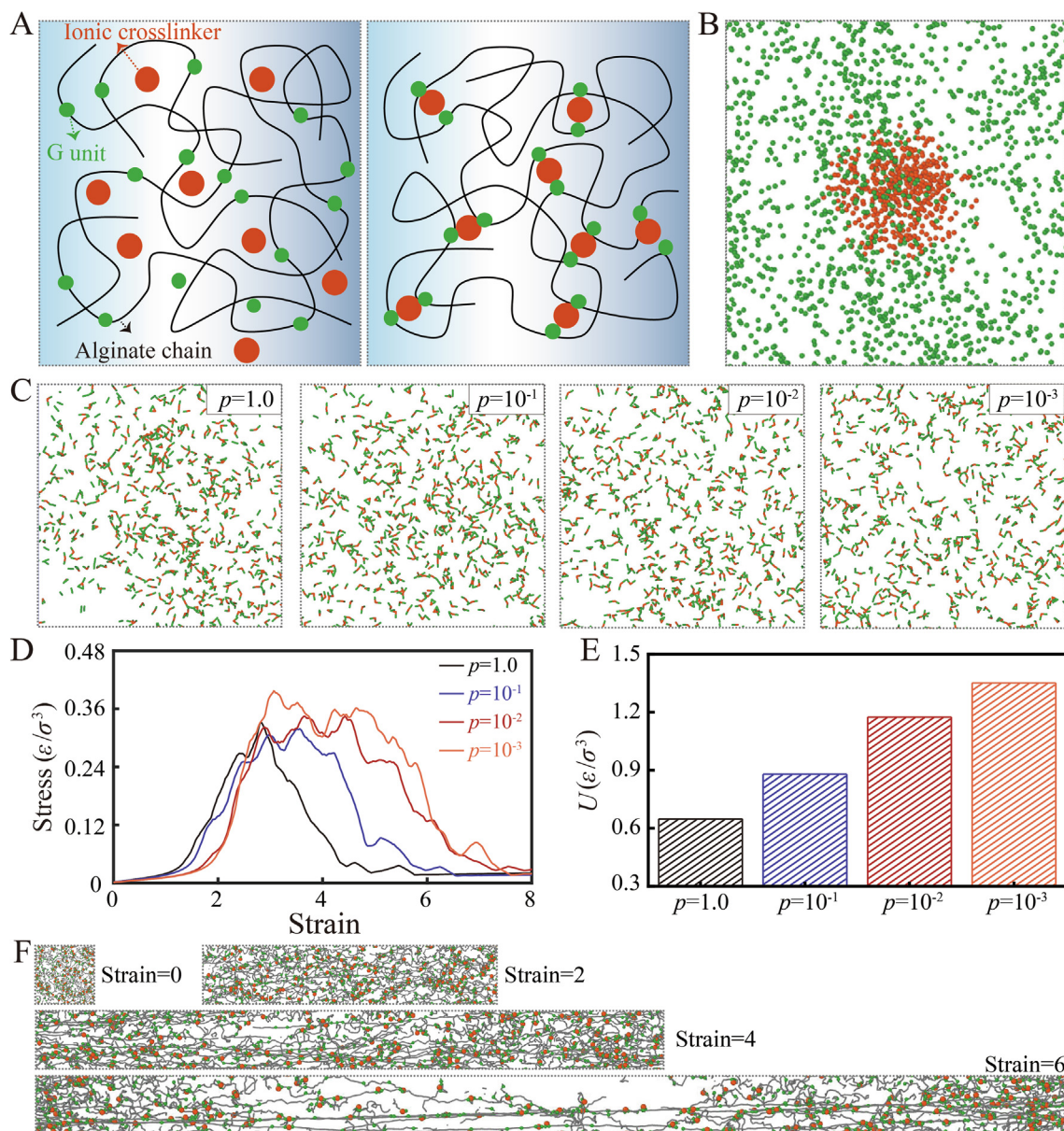


Fig. 3. Effect of ionic crosslinking rate on the mechanical properties of hydrogels. (A) Illustration of the model system. Black lines indicate the polymer (alginate) chains, green spheres indicate the G units in alginate chains and red spheres indicate the ionic crosslinker (Ca^{2+}). (B) Initial distribution of crosslinkers in the model system. These crosslinkers are arranged in eight clusters at the beginning of the simulations, and for clarity, only one eighth of the simulation box and one cluster are shown. (C) Snapshots of the distribution of crosslinks in the hydrogel for $p = 1.0, 10^{-1}, 10^{-2}$ and 10^{-3} , respectively. (D) Stress–strain behavior and (E) energy per unit volume before failure of the hydrogel. The toughness of the hydrogel is characterized by the area under the stress–strain curve (the energy per unit volume before failure, U). (F) Snapshots of the fracture process of the model hydrogel for $p = 10^{-3}$. p represents the reaction probability when one crosslinker encounters the G unit. (For interpretation of the references to colour in this figure legend, the reader is referred to the web version of this article.)

ness. These hydrogels can be stretched to 26 times their original length without rupture (Fig. 4A). When a notch was created in the side of a hydrogel and then the notched hydrogel was pulled to a stretch of 22, the notch was dramatically blunted and remained stable (Fig. 4B).

The mechanical properties of these alginate- Ca^{2+} /PAAm DN hydrogels with various weight ratios of $\text{Na}_4\text{P}_2\text{O}_7$ to CaSO_4 (Figure 4 and Table S1) were studied systematically. When the weight ratio of $\text{Na}_4\text{P}_2\text{O}_7$ to CaSO_4 increases from 14.12 wt.% to 37.62 wt.%, the tensile strength decreases gradually from 260.40 ± 11.55 kPa to 166.02 ± 6.25 kPa (Figures 4C and D, Table S1). In contrast, with increasing weight ratio of $\text{Na}_4\text{P}_2\text{O}_7$ to CaSO_4 , the critical stretch at rupture and the fracture energy both exhibit a trend of increasing first and then decreasing (Figures 4E and F, Table S1). When

the weight ratio of $\text{Na}_4\text{P}_2\text{O}_7$ to CaSO_4 is below 18.81 wt.%, the fracture energy increases with increasing $\text{Na}_4\text{P}_2\text{O}_7$ to CaSO_4 ratio. As shown in Figure 2C, a higher weight ratio of $\text{Na}_4\text{P}_2\text{O}_7$ to CaSO_4 means a lower ionic reaction rate. From the molecular dynamics simulations (Fig. 3), it has been proven that a lower ionic reaction rate results in better homogeneity, further leading to improved mechanical properties of the hydrogels, which can explain the increasing trend of mechanical properties with the weight ratio of $\text{Na}_4\text{P}_2\text{O}_7$ to CaSO_4 before reaching 18.81 wt.% (Fig. 4E and F).

The fracture energy declines with a further increase in the ratio, which can be explained by the two adverse effects resulting from the excessive amount of $\text{Na}_4\text{P}_2\text{O}_7$. First, the ionic crosslinking density is lowered due to the excessive consumption of CaSO_4 by $\text{Na}_4\text{P}_2\text{O}_7$. Second, excessive $\text{Na}_4\text{P}_2\text{O}_7$ may cause the ionic crosslinking

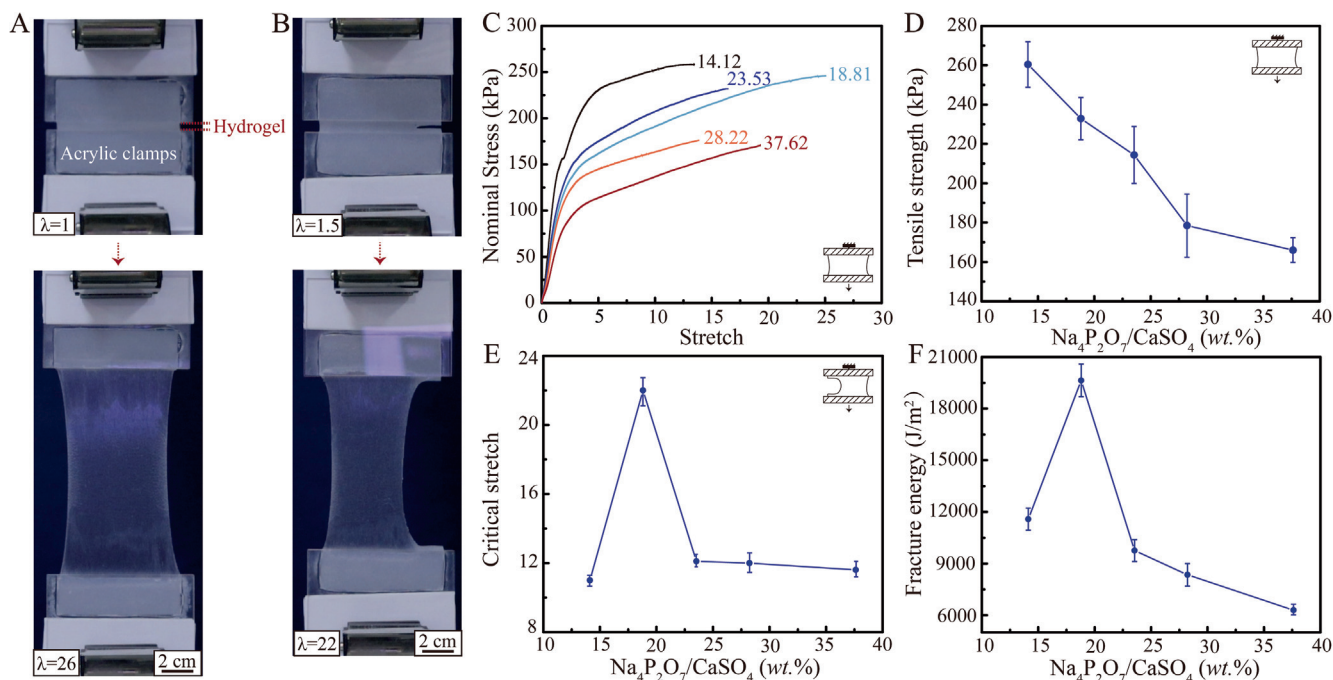


Fig. 4. Highly stretchable and notch-insensitive alginate-Ca²⁺/PAAm DN hydrogel. (A) Hydrogel stretched to 26 times its initial length in a tensile machine. The stretch, λ , is defined by the distance between the two acrylic clamps when the hydrogel is deformed, divided by the distance when the hydrogel is undeformed. (B) Notched hydrogel stretched to 22 times its initial length. (C) Stress-strain curves of unnotched alginate-Ca²⁺/PAAm DN hydrogel with various weight ratios of Na₄P₂O₇ to CaSO₄. (D) Tensile strength calculated from stress-strain curves plotted against weight ratios. (E) Critical stretch, λ_c , for notched hydrogels measured by pulling the hydrogel to rupture. (F) Fracture energy as a function of weight ratio. Error bars show standard deviations with sample size $n \geq 6$. Water content was 86.00 wt.%.

rate to be too slow, and thus, the gelation time to be too long. An excessively prolonged gelation time will further lead to the sedimentation of CaSO₄, which will inevitably decrease the homogeneity. The declined ionic crosslinking density and homogeneity finally contribute to the lowered fracture energy. Thus, the critical stretch at rupture and the fracture energy reach maxima of 22.00 ± 0.32 (Fig. 4E and Table S1) and $19,638 \pm 947$ J/m² (Fig. 4F and Table S1) at a weight ratio of 18.81 wt%, respectively. The fracture energy of $19,638 \pm 947$ J/m² is notably larger than the previously reported value of ~ 9000 J/m² obtained by the conventional method [14], which clearly demonstrates the effectiveness of our strategy in toughening alginate-Ca²⁺/PAAm DN hydrogels. In addition to the weight ratio of Na₄P₂O₇ to CaSO₄ (Fig. 4), the weight ratios of CaSO₄ to alginate (Figure S6 and Table S2) and AAm to AAm plus alginate (Figure S7 and Table S3) and water content (Figure S8 and Table S4) also strongly affect the mechanical behavior of the alginate-Ca²⁺/PAAm DN hydrogels. More details can be found in the Supplementary Materials.

3.4. Extensibility and generality of *in situ* inhibition method

The extensibility is greatly enhanced due to various alternative soluble salts to Na₄P₂O₇. As shown in Fig. 5A, soluble salts, such as Na₂CO₃, Na₂C₂O₄ and C₆H₅Na₃O₇, may become alternatives. The appearance of the hydrogels obtained by the introduction of Na₂CO₃ or Na₂C₂O₄ is smooth, similar to that of Na₄P₂O₇. However, the appearance of the hydrogels formed by C₆H₅Na₃O₇ is similar to that without any soluble salts. These results suggested that Na₂CO₃ and Na₂C₂O₄ may be effective while C₆H₅Na₃O₇ may be ineffective in decreasing the ionic crosslinking rate.

The inhibition effects resulting from these soluble salts were further verified by measuring the viscosity variation during gelation of the pre-gel solutions. As shown in Fig. 5B, the initial viscosities of the pre-gel solution with Na₂CO₃, Na₄P₂O₇ and Na₂C₂O₄ are only 4687–5729 cp, i.e., lower than that of the pre-gel solution

without any soluble salts ($\sim 41,668$ cp). Conversely, the initial viscosity of the pre-gel solution with C₆H₅Na₃O₇ is almost the same as that of the pre-gel solution without any soluble salts. These results clearly demonstrate that Na₂CO₃ and Na₂C₂O₄ can be alternatives to Na₄P₂O₇ in decreasing the ionic crosslinking rate, while C₆H₅Na₃O₇ is completely ineffective. The effectiveness of these salts may be justified by the solubilities of the inhibitors formed by their reaction with CaSO₄. The solubilities of these inhibitors formed by Na₄P₂O₇, Na₂CO₃, Na₂C₂O₄ and C₆H₅Na₃O₇ are $\sim 2.3 \times 10^{-5}$, $\sim 5.29 \times 10^{-4}$, $\sim 6.7 \times 10^{-4}$ and ~ 0.1 g/100 g, respectively. It can be seen that the higher the insolubility, the greater the reduction in viscosity and thus the lower the ionic crosslinking rate (Fig. 5B). For C₆H₅Na₃O₇, the solubility of its corresponding inhibitor is comparable to that of CaSO₄ (~ 0.2 g/100 g), which can explain its ineffectiveness in decreasing the ionic crosslinking rate. Therefore, the inhibition effects can be improved by adopting salts that can *in situ* generate a more insoluble inhibitor around ionic crosslinker.

The mechanical properties of these alginate-Ca²⁺/PAAm DN hydrogels after introducing the soluble salts were also investigated in detail (Fig. 5C-E and Table S5). These hydrogels have ultrahigh fracture energies ranging from $14,706 \pm 14$ J/m² to $19,638 \pm 947$ J/m², which outperform most tough DN hydrogels reported previously, including gelatin-PAAm, gelatin- κ -carrageenan-PAAm, κ -carrageenan-PAAm, agar-PAAm and alginate-Ca²⁺/PAAm (Fig. 5F) [10,14,18,22,30–33]. To our knowledge, the fracture energy of $19,638 \pm 947$ J/m² is the highest value reported for hydrogels with high water contents (~ 86 wt.%).

For our *in situ* inhibition method, there are various soluble salts (like Na₄P₂O₇, Na₂CO₃, Na₂C₂O₄, etc) available to *in situ* generate efficient inhibitors, which can greatly improve the extensibility of our strategy. Based on its mechanism, this method can be extended to other ionically crosslinked networks, like κ -carrageenan-Zr⁴⁺, chitosan-SO₄²⁻, chitosan-cit³⁻ and chitosan-Ag⁺. As a result, our strategy has significant potential to become a general method to toughen DN hydrogels containing ionically crosslinked networks.

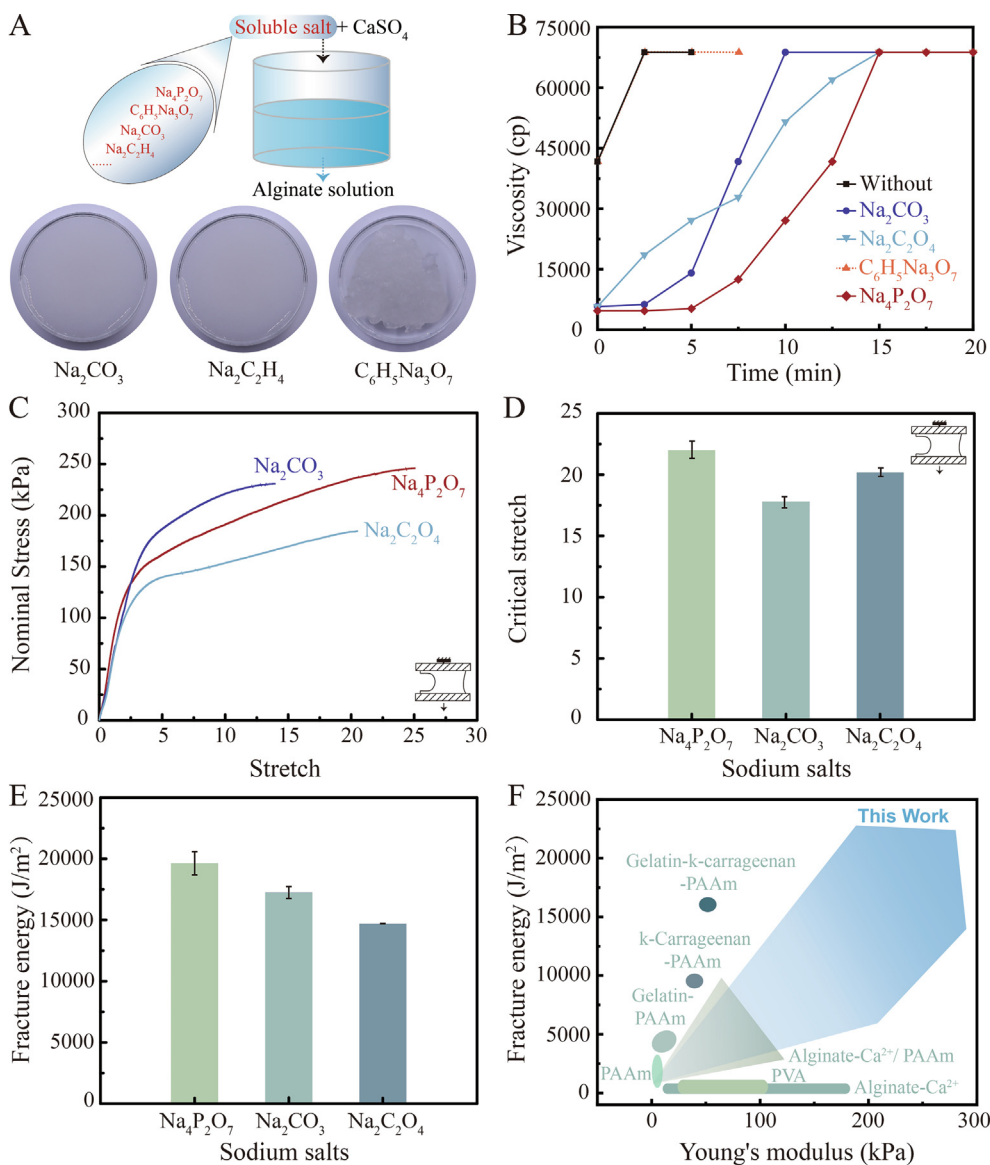


Fig. 5. Extensibility and generality of the *in situ* inhibition method. (A) Photographs of alginate-Ca²⁺ SN hydrogels prepared by the *in situ* inhibition method with various soluble salts of Na₂CO₃, Na₂C₂O₄ and C₆H₅Na₃O₇. (B) Viscosity-time curve of pre-gel solutions for alginate-Ca²⁺ SN hydrogels with different soluble salts. (C) Stress-strain curves of unnotched alginate-Ca²⁺/PAAm DN hydrogel with various sodium salts. (D) Critical stretch, λ_c, for notched hydrogels, measured by pulling the hydrogels to rupture. (E) Fracture energy as a function of different salts. Error bars show standard deviation with sample size n ≥ 6. The weight ratios of these soluble salts to CaSO₄ were fixed at 18.81 wt.%. (F) Material property chart of the fracture energy versus Young's modulus for various hydrogels.

4. Conclusions

In this work, a new *in situ* inhibition method has been proposed to decrease the ionic crosslinking rate effectively and controllably, and thus, toughen DN hydrogels. This was achieved by generating a substance known as an inhibitor *in situ* to form a physical barrier around the ionic crosslinker, which could impede the release of crosslinking ions. A variety of soluble salts are available to generate efficient inhibitors and the solubility of the inhibitor strongly affects the inhibition effect. A reduced ionic crosslinking rate helps to improve the homogeneity and overall ionic crosslinking density, and further enhances the mechanical properties of DN hydrogels, as verified by molecular dynamics simulations. The alginate-Ca²⁺/PAAm DN hydrogels prepared through our strategy display superior mechanical properties. The fracture energy is up to 19,638 ± 947 J/m², which, to our knowledge, is the highest value reported for hydrogels with high water contents. Our strategy has the advantages of simplicity, generality, high performance,

near net-shape forming, sustainability, industrial friendliness and so on. These advantages make it suitable for the preparation of tough hydrogels that can meet more demanding load-bearing requirements.

CRedit authorship contribution statement

Nannan Jian: Methodology, Investigation, Writing – original draft. **Jiuling Wang:** Investigation, Methodology, Writing – original draft. **Lei Zuo:** Writing – review & editing. **Kai Zhang:** Writing – review & editing, Methodology, Project administration, Funding acquisition.

Data availability

Data will be made available on request.

Declaration of Competing Interest

The authors declare that they have no known competing financial interests or personal relationships that could have appeared to influence the work reported in this paper.

Acknowledgements

This work was supported by the National Natural Science Foundation of China (Grants Nos. 11991030, 12272041, 12202055 and 12202057).

Data and materials availability

All data are available in the main text and/or the [Supplementary Materials](#).

Appendix A. Supplementary data

Supplementary data to this article can be found online at <https://doi.org/10.1016/j.matdes.2022.111522>.

References

- [1] Y. Xue, J. Zhang, X. Chen, J. Zhang, G. Chen, K. Zhang, J. Lin, C. Guo, J. Liu, Trigger-detachable hydrogel adhesives for bioelectronic interfaces, *Adv. Funct. Mater.* 31 (2021) 2106446, <https://doi.org/10.1002/adfm.202106446>.
- [2] L. Zhang, C. Wan, J. Su, C. Zhang, S. Wei, W. Tian, X. Liu, W. Cheng, X. Li, X. Li, X. Guo, K.-T. Yong, Y. Wu, A dual-crosslinked self-healing and antibacterial nanocellulose hydrogel for monitoring of human motions, *Mater. Design* 215 (2022), <https://doi.org/10.1016/j.matdes.2022.110464> 110464.
- [3] H. Yuk, B. Lu, X. Zhao, Hydrogel bioelectronics, *Chem. Soc. Rev.* 48 (2019) 1642–1667, <https://doi.org/10.1039/c8cs00595h>.
- [4] C. Chen, H. Qin, H. Cong, S. Yu, A Highly stretchable and real-time healable supercapacitor, *Adv. Mater.* 31 (2019) 1900573, <https://doi.org/10.1002/adma.201900573>.
- [5] H. Lin, J. Tan, J. Zhu, S. Lin, Y. Zhao, W. Yu, H. Hojajji, B. Wang, S. Yang, X. Cheng, Z. Wang, E. Tang, C. Yeung, S. Emaminejad, A programmable epidermal microfluidic valving system for wearable biofluid management and contextual biomarker analysis, *Nat. Commun.* 11 (2020) 4405, <https://doi.org/10.1038/s41467-020-18238-6>.
- [6] B.V. Slaughter, S.S. Khurshid, O.Z. Fisher, A. Khademhosseini, N.A. Peppas, Hydrogels in regenerative medicine, *Adv. Mater.* 21 (2009) 3307–3329, <https://doi.org/10.1002/adma.200802106>.
- [7] A.P. Nowak, V. Breedveld, L. Pakstis, B. Ozbas, D.J. Pine, D. Pochan, T.J. Deming, Rapidly recovering hydrogel scaffolds from self-assembling diblock copolypeptide amphiphiles, *Nature* 417 (2002) 424–428, <https://doi.org/10.1038/417424a>.
- [8] J. Meng, F. Boschetto, S. Yagi, E. Marin, T. Adachi, X. Chen, G. Pezzotti, S. Sakurai, H. Yamane, H. Xu, Melt-electrowritten poly(L-lactic acid)- and bioglass-reinforced biomimetic hydrogel for bone regeneration, *Mater. Design* 219 (2022), <https://doi.org/10.1016/j.matdes.2022.110781> 110781.
- [9] H. Yuk, S. Lin, C. Ma, M. Takaffoli, N.X. Fang, X. Zhao, Hydraulic hydrogel actuators and robots optically and sonically camouflaged in water, *Nat. Commun.* 8 (2017) 14230, <https://doi.org/10.1038/ncomms14230>.
- [10] C. Li, S. Zheng, X. Hao, W. Hong, Q. Zheng, Z. Wu, Spontaneous and rapid electro-actuated snapping of constrained polyelectrolyte hydrogels, *Sci. Adv.* 8 (2022) eabm9608, <https://doi.org/10.1126/sciadv.abm9608>.
- [11] F. Oveissi, D.F. Fletcher, F. Dehghani, S. Naficy, Tough hydrogels for soft artificial muscles, *Mater. Design* 203 (2021), <https://doi.org/10.1016/j.matdes.2021.109609> 106609.
- [12] P. Zhang, I.M. Lei, G. Chen, J. Lin, X. Chen, J. Zhang, C. Cai, X. Liang, J. Liu, Integrated 3D printing of flexible electroluminescent devices and soft robots, *Nat. Commun.* 13 (2022) 4775, <https://doi.org/10.1038/s41467-022-32126-1>.
- [13] K. Zhang, C. Ma, Q. He, S. Lin, Y. Chen, Y. Zhang, N.X. Fang, X. Zhao, Metagel with broadband tunable acoustic properties over air-water-solid ranges, *Adv. Funct. Mater.* 29 (2019) 1903699, <https://doi.org/10.1002/adfm.201903699>.
- [14] J.-Y. Sun, X. Zhao, W.R.K. Illeperuma, O. Chaudhuri, K.H. Oh, D.J. Mooney, J.J. Vlassak, Z. Suo, Highly stretchable and tough hydrogels, *Nature* 489 (2012) 133–136, <https://doi.org/10.1038/nature11409>.
- [15] J. Gong, Why are double network hydrogels so tough?, *Soft Matter* 6 (2010) 2583–2590, <https://doi.org/10.1039/b924290b>.
- [16] J. Gong, Y. Katsuyama, T. Kurokawa, Y. Osada, Double-network hydrogels with extremely high mechanical strength, *Adv. Mater.* 15 (2003) 1155–1158, <https://doi.org/10.1002/adma.200304907>.
- [17] H. Yu, C. Li, M. Du, Y. Song, Z. Wu, Q. Zheng, Improved toughness and stability of kappa-carrageenan/polyacrylamide double-network hydrogels by dual cross-linking of the first network, *Macromolecules* 52 (2019) 629–638, <https://doi.org/10.1021/acs.macromol.8b02269>.
- [18] J. Li, W.B.K. Illeperuma, Z. Suo, J.J. Vlassak, Hybrid hydrogels with extremely high stiffness and toughness, *ACS Macro Lett.* 3 (2014) 520–523, <https://doi.org/10.1021/mz5002355>.
- [19] T. Li, G. Li, Y. Liang, T. Cheng, J. Dai, X. Yang, B. Liu, Z. Zeng, Z. Huang, Y. Luo, T. Xie, W. Yang, Fast-moving soft electronic fish, *Sci. Adv.* 3 (2017) e1602045.
- [20] Y. Han, Q. Zeng, H. Li, J. Chang, The calcium silicate/alginate composite: Preparation and evaluation of its behavior as bioactive injectable hydrogels, *ACS Biomater.* 9 (11) (2013) 9107–9117.
- [21] T.T. Pham, P.L. Tran, C.D. Phung, H.T. Nguyen, C.H. Nguyen, C.S. Yong, J.O. Kim, S. Yook, J.-H. Jeong, Surface-triggered in situ gelation for tunable conformal hydrogel coating of therapeutic cells and biomedical devices, *Adv. Funct. Mater.* 31 (2021) 2010169, <https://doi.org/10.1002/adfm.202010169>.
- [22] X. Sun, L. Ye, H. Liang, Extremely stretchable and tough hybrid hydrogels based on gelatin, kappa-carrageenan and polyacrylamide, *Soft Matter* 17 (2021) 9708–9715, <https://doi.org/10.1039/d1sm01135a>.
- [23] Y. Yin, N. Bertin, Y. Wang, Z. Bao, W. Cai, Topological origin of strain induced damage of multi-network elastomers by bond breaking, *Extreme Mech. Lett.* 40 (2020), <https://doi.org/10.1016/j.eml.2020.100883> 100883.
- [24] A.P. Thompson, H.M. Aktulga, R. Berger, D.S. Bolintineanu, W.M. Brown, P.S. Crozier, P.J. in 't Veld, A. Kohlmeyer, S.G. Moore, T.D. Nguyen, R. Shan, M.J. Stevens, J. Tranchida, C. Trott, S.J. Plimpton, LAMMPS—a flexible simulation tool for particle-based materials modeling at the atomic, meso, and continuum scales, *Comput. Phys. Commun.* 271 (2022) 108171.
- [25] J. Tauber, L. Rovigatti, S. Dussi, J. van der Gucht, Sharing the load: Stress redistribution governs fracture of polymer double networks, *Macromolecules* 54 (2021) 8563–8574, <https://doi.org/10.1021/acs.macromol.1c01275>.
- [26] J. Wang, T.C. O'Connor, G.S. Grest, T. Ge, Superstretchable elastomer from cross-linked ring polymers, *Phys. Rev. Lett.* 128 (2022), <https://doi.org/10.1103/PhysRevLett.128.237801> 237801.
- [27] C.W. Barney, Z. Ye, I. Sacligil, K.R. McLeod, H. Zhang, G.N. Tew, R.A. Riggelman, A.J. Crosby, Fracture of model end-linked networks, *P. Natl. Acad. Sci. U.S.A.* 119 (2022) e2112389119, <https://doi.org/10.1073/pnas.2112389119>.
- [28] R.S. Rivlin, A.G. Thomas, Rupture of rubber. 1. characteristic energy for tearing, *J. Polym. Sci.* 10 (1953) 291–318, <https://doi.org/10.1002/pol.1953.120100303>.
- [29] S. Zhou, A. Bismarck, J.H.G. Steinke, Ion-responsive alginate based macroporous injectable hydrogel scaffolds prepared by emulsion templating, *J. Mater. Chem. B* 1 (2013) 4736–4745, <https://doi.org/10.1039/c3tb20888e>.
- [30] W.C. Ballance, V. Karthikeyan, I. Oh, E.C. Qin, Y. Seo, T. Spearman-White, R. Bashir, Y. Hu, H. Phillips, H. Kong, Preoperative vascular surgery model using a single polymer tough hydrogel with controllable elastic moduli, *Soft Matter* 16 (2020) 8057–8068, <https://doi.org/10.1039/d0sm00981d>.
- [31] P. Peng, J. Zhou, L. Liang, X. Huang, H. Lv, Z. Liu, G. Chen, Regulating thermogalvanic effect and mechanical robustness via redox ions for flexible quasi-solid-state thermocells, *Nano-Micro Lett.* 14 (2022) 81, <https://doi.org/10.1007/s40820-022-00824-6>.
- [32] S. Liu, L. Li, Recoverable and self-healing double network hydrogel based on kappa-carrageenan, *ACS Appl. Mater. Interfaces* 8 (2016) 29749–29758, <https://doi.org/10.1021/acsami.6b11363>.
- [33] X. Lu, C.Y. Chan, K.I. Lee, P.F. Ng, B. Fei, J.H. Xin, J. Fu, Super-tough and thermo-healable hydrogel-promising for shape-memory absorbent fiber, *J. Mater. Chem. B* 2 (2014) 7631–7638, <https://doi.org/10.1039/c4tb01289e>.